Experimental Preliminary Analysis of the Fluid Drag Effect in Rapid and Long-runout Flowlike Landslides

Yang Gao (737263992@qq.com)
Institute of Geo-Mechanics, Chinese Academy of Geo-Sciences https://orcid.org/0000-0002-7098-0476
Haoyuan Gao
Chinese Academy of Geological Sciences Institute of Geomechanics
Bin Li
Chinese Academy of Geological Sciences Institute of Geomechanics
Tongyao Wei
Chinese Academy of Geological Sciences Institute of Geomechanics
Zhuang Li
Chinese Academy of Geological Sciences Institute of Geomechanics

Research Article

Keywords: Flowlike landslides, Drag force, Experimental Analysis,Two-phase

Posted Date: June 21st, 2021

DOI: https://doi.org/10.21203/rs.3.rs-616229/v1

Experimental Preliminary Analysis of the Fluid Drag Effect in Rapid and Long-runout Flowlike Landslides

Yang Gao [1,2], Haoyuan Gao [1,2], Bin Li [1,2,3], Tongyao Wei [3], Zhuang Li [3]

1. Institute of Geo-Mechanics, Chinese Academy of Geo-Sciences, CGS, Beijing, China;

2. Key Laboratory of Active Tectonics and Crustal Stability Assessment, Beijing, China;

3. Chang'an University, Xian, China

Abstract: During a landslide, the multi-phase nature of landslide debris defines its mobility. Eventually, frictional forces cause the slide energy to dissipate, and contact forces transmit the energy into nearby material. To analyze the dynamic characteristics of high-velocity long-runout landslides, we conducted flume model tests to empirically determine the mobility characteristics of flow-like landslides with various slide materials. Our conclusions are as follows: (1) Liquid-phase flow-like landslides are highly mobility and have long runout; solid-phase flow-like landslides are highly destructive because of their higher kinetic energy; and two-phase flow-like landslides are both highly mobility. (2) During a two-phase flow-like landslide, the mobility ability of the liquid-phase material is stronger than that of the solid-phase material; when the liquid slide volume fraction is sufficiently large, the liquid phase exerts a drag force on the solid phase. (3) Various liquids exert different drag effects on the solid; the solid-liquid velocity difference and the liquid viscosity determine the drag intensity and the mobility and depositional characteristics of the landslide.

Keywords：Flowlike landslides; Drag force; Experimental Analysis;Two-phase

1. INTRODUCTION

A landslide occurs when rock, debris, and/or soil falls down a slope under the influence of gravity (Valagussa et al., 2019). During a landslide, there are dynamic interactions between the slide material and other media in various phases (solid, gas, and liquid) that shape the mobility characteristics of the landslide. While frictional forces cause the energy of the slide to dissipate, contact forces transfer the energy from the slide material to nearby media. All energy loss during a landslide is caused by friction (Sassa, 1988). Within a landslide, internal energy transfer between the debris particles supplies the front part of the debris flow with energy from the rear part of the slide, which enables the slide to achieve high velocities and, consequently, long runouts (Eisbacher, 1979; Gassen and Cruden, 1990; Ge et al., 2020). Previous studies proposed that a gas buoyancy force exists at the bottom of a landslide that reduces the friction of the slide and increases both the slide runout distance and the amount of damage imparted by the landslide (Kent, 1966; Shreve, 1986; Habib, 1975). Landslide liquefaction effect occurs when a saturated slide shears rapidly with respect the boundary layer, which results in a high pore water pressure in the liquid sliding material. This excessive pore pressure decreases the effective stress between adjacent solid particles, reduces the kinetic friction of the landslide, and increases the slide runout distance (Castro, 1975; Evans, 2001; Sassa et al., 2004; Iverson et al, 2016).

When the liquid volume fraction of a slide is sufficiently large, it results in a two-phase (solid-liquid) flow slide. In this type of slide, the solid-liquid interactions generate a buoyancy force that is oriented perpendicular to the slide mobility direction and a flow drag force that is oriented parallel to the slide mobility direction. These landslides, which are characterized by high velocities, long runouts, complex dynamics, and flow-like mobility characteristics, are collectively known as flow-like landslides. These catastrophic landslide hazards pose a significant threat to nearby

communities (Varnes, 1978; Hutchinson, 1988; Hungr et al., 2001).

Because it is difficult to accurately characterize the dynamic behavior of a landslide by observing it after the fact, physical models are often employed to study these flow-like landslides (Bedford and Drumheller, 1983; Johnson, 1990; Iverson, 1997; Iverson and Denlinger, 2001). Using glass beads as the sliding material, Savage and Hutter (1989) investigated the basal resistance model of the granular flow in collapsing rock, snow, and ice masses. Okura et al. (2002) explored the landslide instability process using a large flume model and concluded that a landslide slides down the slope because high excess pore water pressure is generated at the toe of the slope. Based on the results of numerous laboratory experiments related to landslide debris flows, Iverson (1997, 2001, 2003, 2009, 2011) concluded that pore water pressure and landslide path roughness are the key factors that determine the landslide runout. Sassa (1988, 1998, 2000, 2004) maintained that the ring shear test, used in conjunction with numerical simulations (specifically the RAPID software), results in the most accurate reproduction of the landslide mobility process. Huang (2013, 2014) used ring shear tests and numerical simulations to investigate the mobility of flow-like landslides. Ahmadipur et al. (2019) investigated the effect of basal friction on the velocity and impact force of flow-like landslides using flume tests. While many studies explore flow-like landslides using physical models, most of these studies focus on modeling the solid-solid interactions in these landslides. However, because the basal friction and the impact force are affected by the pore water pressure in the landslide boundary layer, it is necessary to investigate the dynamic characteristics of two-phase landslides.

Of the eleven distinct types of landslide flows (Varnes, 1978; Hungr, 2014), the most important flow types are the debris flow (e.g. the Zhouqu landslide (Tang et al, 2011)), the debris avalanche (e.g. the Jiweishan landslide (Yin et al, 2010)), the debris flood (e.g. the Vancouver

landslide (Hungr et al, 2001)), the earth flow (e.g. the Yining landslide (Yang et al, 2019)), and the mud flow (e.g. the Shenzhen landslide (Gao et al, 2019)). Some of these terms, such as debris avalanche, earth flow, and peat flow, refer to single-phase (solid or liquid) medium landslides, while other flow types, such as debris flow and debris flood, are two-phase landslides defined by the presence of a free liquid. In this study, we conducted flume model tests to quantify the mobility characteristics of flow-like landslides composed of different materials. The objective of this paper is to approve important role of fluid drag effect in rapid and long-runout flowlike landslides, when the liquid volume fraction of a two-phase landslide is sufficiently large. In the remainder of the manuscript we describe the series of flume model tests conducted on two-phase materials of flow like landslide, various liquids drag test on the solid to achieve this objective.

2. EXPERIMENTAL STUDY

2.1 Test objectives and framework

Using two sets of flume tests, we observed the mobility characteristics of solid, liquid, and solid-liquid landslides, analyzed the mobilities of different phase media, and determined how the drag effects of various liquids control the mobility characteristics of two-phase landslides. In the first set of flume tests, we created slides with varying proportions of liquid and solid debris to assess how the slide material affects the landslide mobility and deposition. In the second set of flume tests, we used three different slide materials (gravel, gravel with mud, and gravel with water) to determine how the drag created by different liquid phases (mud and water) affects the solid phase (gravels). The initial slide material, limestone debris and clay mud, is an accurate analog for real landslide material.

2.2 Test site layout

Flume equipment: To facilitate omnidirectional observation of the flume test, we used a

transparent side plate that was marked with grid lines. The flume dimensions are 300 cm × 50 cm × 50 cm (length × width × side plate height). The rest of the chute consisted of a stainless-steel bottom plate and a 50 cm × 50 cm × 50 cm slide hopper that was closed and undrained. The angle of inclination is uniformly selected as 20°. A hydraulic switch-type baffle plate was installed at the outlet of the hopper. An adjustable laser rangefinder was installed directly above the flume.

Data recording equipment: To record the deposition state of the slide after a flume test, we placed a high-speed camera at the front end of the bottom plate. In order to observe the microscopic characteristics of the gravel landslide in real time, we placed high-speed cameras at the front of the bottom plate, on the sides of the flume, above the flume, and inside the flume.

2.3 Sample preparation

The three main materials used in the chute tests were pure water, limestone gravel with a particle size of 20–30 mm (Fig. 2a), and viscous mud consisting of water and fine-grained soil with a clay particle size of 0.005–0.05 mm, (Fig. 2b).

We prepared six different slide materials (Table 1):

- Test T-01: 100 kg of air-dried limestone gravel with a particle size of 20–30 cm
- Test T-02: 50 kg of mud with a soil-water ratio of 1:2 that was poured into 50 kg of gravel, completely filling the spaces between individual pieces of gravel
- Test T-03: 100 kg of mud with a soil-water ratio of 1:2
- Test T-04: 200 kg of limestone gravel
- Test T-05: 100 kg of water poured onto 100 kg of limestone gravel
- Test T-06: 100 kg of mud with a soil-water ratio of 1:2 poured into 100 kg of limestone

2.4 Test process

After loading the appropriate slide material, we used the hydraulic control valve to lift the baffle plate at the front of the hopper, releasing the landslide material. We used multiple high-speed cameras to record the evolution of the landslide mobility and deposition. The deposition state of the post-sliding landslide was captured using a high-speed camera.

We analyzed the photographic images to investigate how the different liquids affected the drag force experienced by the gravel and to determine the extent to which the slide material controls the runout distance. For the slides with water as the fluid medium, the impact velocity of the slide and pressure differences in the water caused the back of the slide to rapidly catch up to the front of the slide. For the slides with mud as the fluid medium, the front, middle, and rear sections of the gravel largely stayed in the same relative positions throughout the landslide due to the drag effect. Using high-speed camera to record the front of the sliding body to different positions at different times. We can calculate the velocity and acceleration of the gravel.

3. RESULTS

In this study, we devised two different types of experiments. In the first set of experiments, solid gravel, mud, and a mixture of mud and gravel slid freely in the flume (which has an inclination of 20°). These experiments were undertaken so that we could better understand how the slide material affects the sliding distance, depositional characteristics, and the mobility velocity and acceleration. In the second set of experiments, solid gravel, a mixture of mud and gravel, and a mixture of water and gravel freely down the same inclined flume. We then analyzed the sliding distance, depositional characteristics, and the mobility velocity and acceleration for each slide to determine how the drag force experienced by the slide material was affected by the presence of different fluids. Through literature reading and experimental observations, high pore

water pressure is only true for materials with a void ratio higher than the void ratio at critical state at the sliding main body current effective confining stress(Jefferies and Been, 2019). Through literature gathering and experimental observations(Park, et al. 2004; Peker and Helvaci, 2011; Shi, et al. 2017), the drag force plays a significant role to compare the pore water pressure, when the fluid volume fraction and gravel pore ratio in two-phase flow are large enough.

3.1 The first set of tests: solid, liquid, and solid-liquid two-phase flow

For these three experiments, we placed ~100 kg of materials, T-01, T-02, and T-03, in the hopper. As each slide slid freely down the inclined flume, we recorded the mobility and depositional characteristics of the landslide.

(1) Experiment T-01: 100 kg of gravel

In this test, not all the slide material left the hopper; only the front particles slid down the flume, leaving most of the gravel inside the hopper. Most pieces of gravel were deposited at the very beginning of the flume, and very few gravel particles made it out of the flume and landed on the bottom plate. Our observations for test T-01 are as follows:

- The solid gravel slid freely in the inclined flume toward the toe of the slope over a period of 4 s.
- The front part of the slide slid down the chute and was deposited at the beginning of the flume. A few pieces of gravel rushed out of the flume and reached the bottom plate.
- Post-sliding measurements indicated that the maximum mobility distance for most of the gravel was ~120 cm, with a few pieces traveling as far as 450 cm.
- According to the high-speed camera images, the maximum mobility velocity of the slide reached ~90 cm/s and it had a maximum acceleration of ~90 cm/s^2. The slide rapidly accelerated and decelerated over time intervals of 1.6 s and 2.4 s, respectively.

(2) Experiment T-02: 100 kg of gravel and mud

Some of the two-phase flow slide quickly exited the flume. Due to the interaction between the mud and the gravel, after the gravel left the hopper, the fluid mud facilitated the mobility of the gravel down the chute. As shown in Figure 3b, the mud fluid exhibited fluid-like behavior by flowing around the obstructions created by gravel clusters in the middle of the leading edge of the slide. As a result, the slide runout was greater than that of the gravel slide. Our observations for test T-02 are as follows:

- The gravel slid down the inclined flume over a period of 13 s.
- The slide flowed around solid obstructions in the middle of the leading edge of the slide; the slide material was deposited throughout the entirety of the chute without actually exiting the chute
- The maximum mobility distance of the slide was 280 cm.
- The maximum mobility velocity of the slide ~120 cm/s and the maximum acceleration was ~120 cm/s^2. The slide exhibited rapid acceleration and a more drawn-out, flow-like deceleration over time intervals of 1.6 s and 11.4 s, respectively.

(3) Experiment T-03: 100 kg of mud fluid

The slide rushed out of the hopper, flowed down the flume and was deposited on the bottom plate. All of the mud slid out of the hopper; the flow-like behavior of the slide was evident in the streamlined, protruding alluvial fan pattern created during the slide depositional phase. Our observations of test T-03 are as follows:

- The mud fluid material slid down the inclined flume over a time period of 5 s.
- The slide material was deposited throughout the entire flume, creating a fluid depositional fan pattern.

- The longest mobility distance of the slide was 380 cm.
- According to the high-speed camera images, the maximum velocity of the slide reached ~190 cm/s and its maximum acceleration was ~190 cm/s^2. As expected for a flow-like landslide, this slide exhibited rapid acceleration and more protracted deceleration over time intervals of 1.8 s and 3.2 s, respectively.

(4) Comparative analysis of the first set of tests

We ran the first set of experiments to explore how the slide material affects the slide dynamics and the depositional state. The results for these three experiments are shown in Table 2.

Based on the analysis of deposition states (Figure 3 and Figure 4), velocity variations (Figure 5a) and acceleration variations (Figure 5b), the solid gravels had a mobility distance of 120 cm, a maximum velocity of 90 cm/s, a maximum acceleration of 90 cm/s^2, the shortest distance, and the smallest sliding force; the fluid mud had a mobility distance of 380 cm, a maximum velocity of 190 cm/s, a maximum acceleration of 190 cm/s^2, the longest distance, and the largest sliding force; the two-phase flow slide had a mobility distance of 280 cm, a maximum velocity of 120 cm/s, a maximum acceleration of 120 cm/s^2, and its mobility velocity and mobility distance were respectively in between those of the above two single-phase flows.

Considering only the solid particles at the leading edge of the slide, we used equation (1) to investigate the effect of friction on the decelerating slide after the leading edge of the slide had reached its maximum velocity. For all of these calculations, we used a flume length of 300 cm. In test T-01, the maximum velocity of the leading edge of the slide (90 cm/s) occurred at a distance of 30 cm; the equivalent kinetic friction coefficient of the solid slide in the deceleration stage is $\mu = 0.51$. In test T-02, the maximum velocity of the leading edge of the slide (120 cm/s)

occurred at a distance of 120 cm. For a deceleration distance of was 160 cm, the equivalent shear friction coefficient is μ = 0.43. For test T-03, the maximum velocity of the leading edge of the slide (190 cm/s) occurred at a distance of 190 cm. For a deceleration distance of 190 cm, the calculated shear friction coefficient of the mud fluid is μ = 0.31. Assuming that the shear friction of the solid is constant, the acceleration provided was also a constant.

$$\frac{1}{2}mv^2 - \frac{1}{2}mv_0{}^2 = mgh - Fl \quad (1)$$

By comparing tests T-01 and T-02, we propose that the presence of the mud fluid reduced the friction coefficient of the slide from 0.51 to 0.43. As shown by the long deceleration distance, the fluid in the two-phase flow slide exerts a pronounced drag effect on the rest of the slide material. Overall, in all three tests, the fluid kinetic friction coefficient was relatively low. The presence of fluid mud contributed to longer runout distances in tests T-02 and T-03 and generally increased the mobility (i.e., the velocity and the mobility distance) of the slide; in the two-phase flow slide, the fluid dragged the gravel further than it traveled in test T-01 in the absence of a fluid phase.

As shown, numerous aspects of a landslide are directly related to the slide material. As expected, the slides that contain fluid slide material have higher velocities than the solid gravel slide, and the mud slide accelerated faster than the two-phase slide. Generally, slide acceleration values and the deceleration distances are inversely proportional to one another. Of the three experiments, ongoing interactions between the fluid and solid phases caused the two-phase slide to have the longest mobility time. Because the solid slide had the largest kinetic friction coefficient, it is much less mobility than the mud slide or the two-phase slide. Overall, the presence of solid slide material increases the impact energy and the destructiveness of the slide, the presence of fluid slide material increases the slide mobility and mobility distance, and the

two-phase flow-like slide exhibits the characteristics of both the solid and liquid phases.

3.2 The second set of tests: the water and mud drag effects

In the second set of experiments, we investigated the drag effect exerted by mud and water on the solid phase. Because water has a lower viscosity than mud, the flow velocity of water is different from that of a solid. To better observe the depositional characteristics of the slide, we increased the mass of the slide to 200 kg for experiments T-04, T-05, and T-06.

(1) Experiment T-04: 200 kg of solid gravel

Due to the interlocking effect between the gravel pieces, as well as the frictional force exerted on the gravel by the flume, most of the gravel remained in the hopper. Some gravel pieces tumbled down the flume, and some of those gravel pieces traversed the flume and were deposited on the bottom plate. Our observations for test T-04 are as follows:

- The solid gravel material slid down the inclined flume over a period of 5 s.
- The front part of the slide, which slid out of the hopper, was largely deposited at the beginning of the flume, with very few gravel pieces tumbling further and landing on the bottom plate.
- Post-sliding measurements indicated that the maximum mobility distance for most of the gravel was ~180 cm, with a few pieces traveling as far as 440 cm. Due to the increased mass of the slide and the energy transfer between the gravel pieces, a larger proportion of the slide left the hopper in test T-04 compared to test T-01.
- The high-speed camera images showed that the maximum mobility velocity of the slide reached 90 cm/s and that its maximum acceleration was ~90 cm/s^2. The solid slide accelerated and decelerated over time periods of 1.8 s and 3.2 s, respectively.

(2) Experiment T-05: 200 kg of mud and gravel

The interaction between the mud and gravel caused the gravel pieces to be dragged down the chute with the mud. Due to this fluid-like mobility, most of the slide left the hopper. Some of the slide material moved down the entire chute and was deposited on the bottom plate. Our observations for test T-05 are as follows:

- The two-phase slide material slid down the inclined flume over a period of 5 s.
- The longest mobility distance of the slide was 380 cm.
- According to the high-speed camera images, the maximum mobility velocity of the slide reached 170 cm/s and its maximum acceleration was 170 cm/s^2. The slide rapidly accelerated and decelerated more slowly over time periods of 1.8 s and 3.2 s, respectively.

(3) T-06: 200 kg of water and gravel

Because of the significant difference in velocity between the water and the gravel, the impact force of the water caused the gravel pieces to travel further down the flume than they did in test T-04. All the slide material left the hopper. While some of the slide stayed in the flume, most of the slide was deposited on the bottom plate, where it formed an alluvial fan. Our observations for test T-06 are as follows:

- The water and gravel slide material slid down the inclined flume over a period of 5 s.
- Because of the difference between the frontal velocity of the slide (i.e., the water velocity) and the backflow velocity (i.e., solid velocity) of the slide, a pressure differential (i.e., the drag effect) arose that caused the slide to travel much further and much faster down the flume than it did in the absence of a fluid phase.
- The high-speed camera images showed that there was a pronounced difference between the mobility of the water and the gravel. The maximum mobility distance of the water was 610 cm, its maximum mobility velocity reached 280 cm/s, and its maximum acceleration was ~240

cm/s^2. The liquid part of the slide accelerated and decelerated over time periods of 2.2 s and 2.8 s, respectively. For the gravel part of the slide, the maximum mobility distance was 580 cm, the maximum mobility velocity reached 260 cm/s, and the maximum acceleration was 200 cm/s^2. The rapid acceleration of the slide and the flow-like deceleration and deposition occurred over time periods of 2.3 s and 2.7 s, respectively.

(4) Comparative analysis

In the second set of tests, we examined the slide mobility, deposition, and drag effects in different two-phase flows.

For test T-04, with a maximum leading edge velocity of 90 cm/s occurring at a distance of 90 cm and a deceleration distance of 90 cm, the kinetic friction coefficient of the slide was μ = 0.41 from equation (1). With a maximum leading edge of 170 cm/s at a distance of 170 cm, a maximum acceleration of 170 cm/s^2, and a deceleration distance of 210 cm, the equivalent shear friction coefficient of the slide in test T-05 was μ = 0.3. With a maximum leading edge velocity of 260 cm/s occurring at a distance of 460 cm, the equivalent friction coefficient for the slide material in test T-06 was μ = 0.16.

The doubling of the slide mass of test T-01 in test T-04 increased both the number of collisions and the energy transfer between gravel pieces. This resulted in a greater slide runout and a reduced slide friction coefficient. Due to the presence of the mud and the water, the friction coefficients of the two-phase slides in tests T-05 and T-06 were smaller than that of the single-phase slide in test T-04. A comparison of tests T-05 and T-06 revealed that the fluid water imparted a larger drag force on the gravel, thereby enhancing the mobility and increasing the velocity and mobility distance of the slide.

Based on these experimental results, we analyzed the drag effects of water and mud on the

gravel (Table 3). In comparing tests T-04 and T-05, we found that the presence of mud decreased the friction coefficient from 0.41 to 0.3, while the presence of water decreased the friction coefficient in from 0.41 (test T-04) to 0.16 (test T-06). Comparison of these three tests indicates that the viscosity of the fluid was the main cause of the drag effect; in the mud and gravel slide, the mud increased the maximum slide velocity by a factor of two. In the water and gravel slide, the drag effect of the water was created by a pressure differential that arose due to the velocity difference between the water and the gravel, resulting in a three-fold increase in the maximum slide velocity. Overall, the drag effect created by the water-gravel velocity difference in test T-06 was greater than that caused by the mud viscosity in test T-05.

Different fluids use different mechanisms to produce the drag effect on the solid slide material. Because water has a low viscosity, it is highly mobility, and the drag mode of the slide was characterized by a pressure differential that was caused by the velocity difference between the water and the gravel. A comparison of tests T-04 and T-06 shows that the velocity variations between the gravel and the water were relatively consistent throughout the deceleration stage, but that the acceleration time period was longer in the presence of water. As such, we conclude that the drag effect was more prominent in the acceleration stage than it was in the deceleration stage in test T-06. In the presence of mud, the drag effect arose due to the mud viscosity. Comparison of tests T-04 and T-05 shows that the velocity variation trends were relatively consistent in the acceleration stage, while the drag effect created by the mud resulted in slide deceleration differences that were much more pronounced. Because the drag effect is present in all two-phase flow-like landslides, it is necessary to incorporate the fluid drag force into landslide models when determining the basal resistance.

4. DISCUSSION

The interaction between fluids and solids is an important topic in fluid dynamics. From the perspective of landslide dynamics, we explored the dynamics of the fluid on the solid debris flow with respect to the drag effect, slide mobility, and slide deposition. There are three ways in which a fluid can act upon the solid material. In the first case, the fluid force that arises is unrelated to the relative mobility between the fluid and the mass; the force will not disappear even if the relative velocity and acceleration are zero (e.g., gravity and buoyancy). In the second case, the fluid force depends on the relative mobility between the fluid and the solid and is oriented in the same direction as the relative mobility of the slide (i.e., the longitudinal force). Examples of this type of force include the drag force, the additional mass force, and the Basset force. In the third case, the fluid force depends on the relative mobility between the fluid and the solid and is oriented perpendicular to the direction of relative mobility (i.e., the lateral force). Examples of this type of force include the lift force, the Magnus force, and the Saffman force(Thevand and Daniel, 2002; Zydak and Klemens, 2007).

Two-phase flow models are based on the mass and momentum balance laws for their fluid and solid constituents. Anderson et al. (1995) considered the influence of the fluid-solid velocity difference and the viscous force on the drag force model and proposed a method of calculating the fluid drag force in a fluid-solid two-phase flow. There are two main analysis methods for two-phase flow models: (1) the particle mobility method, which assumes that the characteristics of fluid mobility are determined by certain fluid mechanical properties, and (2) the empirical method, in which the interaction between the fluid and solid phases is determined experimentally (Jackson, 2000).

In the study of two-phase flow slides, the fluid force experienced by solid particles

immersed in the fluid consists of the horizontal drag force and the vertical lift force. According to the test results, the material properties of the fluid affect the magnitude of the drag force experienced by the solid material because the fluid material properties impact both the mobility velocity and the viscosity. Based on our observations, we employed the fluid drag force equation proposed by Evett et al. (1987) to investigate the dynamics of two-phase landslides. In this equation, the horizontal drag force is related to the velocity difference, the drag coefficient (which is related to the Reynolds number), the fluid density, and the frontal area of the solid:

$$F_D = C_D \frac{1}{2} \rho A (u - v)^2 \tag{8}$$

where C_D is the fluid drag coefficient, u is the fluid mobility velocity, v is the solid mobility velocity, A is the area of the solid particle perpendicular to the flow direction, and ρ is the fluid density.

C_D can be expressed according to the fluid mobility state and the dimensionless Reynolds number. The equation for the Reynolds number, which characterizes the fluid flow, is $Rep=\rho vd/\eta$, where v, ρ, and η are the velocity, density, and viscosity coefficient of the fluid, respectively, and d is a characteristic length. The viscosity η can be obtained in laboratory tests. Depending on the circumstances, C_D is calculated in one of three ways. When the fluid mobility state is characterized by a Navier-Stokes viscous flow (i.e., Rep < 1), C_D = 24/Rep. When the fluid mobility state is characterized by a transition zone (i.e., 1 < Rep < 500), (2) C_D = 18.5/0.6*Rep. When the fluid mobility state is characterized by a Newtonian fluid (i.e., 500 < Rep < 2×10^5), $C_D \approx 0.44$. Furthermore, the shape of the solid particles also affects the drag force of the fluid. After the drag coefficient is obtained, the drag force on solid particles is then calculated using Equation (8).

This equation demonstrates that the cohesive force of the fluid medium, the shape of solid particles, and the velocity difference between the fluid and the solid all affect the drag force. In

our experiments, the drag force is expressed as a pressure, which arises due to the velocity differential between the solid and the fluid, and a viscous force, which arises due to the friction between the fluid and solid particles (i.e., the drag coefficient). Because water has a low viscosity and is highly mobility, it can more easily drag the solid gravel pieces down the flume. The higher viscosity and less mobility mud fluid relied on the fluid drag effect to force the gravel particles to travel down the flume.

5. CONCLUSION

In this study, we conducted flume model tests to explore the mobility, deposition, and drag effect characteristics of flow-like landslides consisting of different materials. Our conclusions are as follows:

(1) Liquid phase flow-like landslides are highly mobility and have long-runout. Solid phase flow-like landslides have higher more kinetic energy and destructive, but mobility are poor. And two-phase flow-like landslides incorporate features from both the liquid and solid phase flow-like landslides.

(2) During a two-phase flow-like landslide, when the liquid volume fraction is sufficiently large, the liquid phase exerts a drag force on the solid phase. Liquids with different properties have different drag effects on the solid slide material. The solid-liquid velocity difference and the liquid viscosity determine the drag intensity and affect the mobility and deposition characteristics of the landslide.

(3) Analysis of the test results reveals that the mobility of a solid-liquid two-phase flow slide can be divided into two characteristic stages: the initial sliding stage and the end deposition stage. When dragged by a fluid with a low viscosity (i.e., water), the slide accelerates due to the

velocity difference between the solid and liquid phases, which creates a pressure differential that drives the slide forward. This velocity difference is more prominent during the initial sliding stage than it is during the deposition stage. When the two-phase slide consists of a fluid with a slightly higher viscosity (i.e., mud), the slide accelerates during the sliding stage due to the viscous friction exerted by the fluid on the solid particles in the two-phase flow.

(4) In our dynamic analysis of the landslide mobility, the frictional resistance of a solid-phase slide is greater than that of a liquid-phase slide. In practice, the frictional resistance of a fluid-solid two-phase slide falls between those two extremes. The drag force of the fluid acting on the solid ultimately leads to high-velocity, long-runout, two-phase landslides. Therefore, the internal interaction forces between the fluid and solid media must be considered in the dynamic analysis of landslides.

ACKNOWLEDGMENTS

We acknowledge support from National Science Foundation of China (Grant No. 41907257), the National Key Research and Development Program of China (2018YFC1504806), Institute of Geo-Mechanics (DZLXJK201901). The authors also thank Letpub Services for English language editing and review services.

REFERENCES

1) Castro, G., 1975. Liquefaction and cyclic deformation of sands. ASCE Journal of Geotechnical Engineering, 101:551-569.

2) Sassa K. (Special Lecture) Geotechnical Model for mobility of Landslides[C]// Proc International Symposium on Landslides. 1988.

3) Yunfeng Ge, Zhou T, Tang H, et al. Influence of the Impact Angle on the mobility and Deposition of Granular Flows. Engineering Geology, 2020.

4) Gassen, W.V., Cruden, D.M., 1990. Momentum transfer and friction in the debris of rock avalanches: Reply. Can. Geotech. J. 27 (5), 698–699.

5) Iverson R M, George D L. Modelling landslide liquefaction, mobility bifurcation and the dynamics of the 2014 Oso disaster. Géotechnique, 2016, 66(3):1-13.

6) Tang C, Triggering conditions and depositional characteristics of a disastrous debris flow event in Zhouqu city, Gansu Province, northwestern China,2011.

7) A. Valagussa, O. Marc, P. Frattini, G.B. Crosta, Seismic and geological controls on earthquake-induced landslide size, Earth and Planetary Science Letters, Volume 506, 2019,Pages 268-281.

8) Eisbacher, G, H. Cliff. collapse and rock avalanches (sturzstroms) in the Mackenzie Mountains, northwestern Canada. Canadian Geotechnical Journal, 1979.

9) Gassen W V, Cruden D M. Momentum transfer and friction in the debris of rock avalanches: Reply. Canadian Geotechnical Journal, 1990, 27(5):698-699.

10) Kent P E. The transport mechanism in catastrophic rock falls. The Journal of Geology, 1966, 74(1): 79-83.

11) Shreve R L, Cloos M. Dynamics of sediment subduction, melange formation, and prism

accretion. Journal of Geophysical Research Solid Earth, 1986, 91(B10).

12) Habib P. Production of gaseous pore pressure during rock slides. Rock Mechanics and Rock Engineering, 1975, 7(4): 193-197.

13) Evans S G, Hungr O, Clague J J. Dynamics of the 1984 rock avalanche and associated distal debris flow on Mount Cayley, British Columbia, Canada; implications for landslide hazard assessment on dissected volcanoes. Engineering Geology, 2001, 61(1): 29-51.

14) Sassa K, Fukuoka H, Wang G, et al. Undrained dynamic-loading ring-shear apparatus and its application to landslide dynamics. Landslides, 2004, 1(1):7-19.

15) Varnes D J. Slope mobility types and processes. Special report, 1978, 176: 11-33.

16) J.N. Hutchinson. General report: morphological and geotechnical parameters of landslides in relation to geology and hydrogeology: Proc 5th International Symposium on Landslides, Lausanne, 10–15 July 1988V1, P3–35. Publ Rotterdam: A A Balkema, 1988. 26(2):88-0.

17) Hungr O, Evans S G, Hutchinson I N. A Review of the Classification of Landslides of the Flow Type. Environmental & Engineering Geoscience, 2001, 7(3): 221-238.

18) A. Bedford, D.S. Drumheller, Theories of immiscible and structured mixtures, International Journal of Engineering Science, Volume 21, Issue 8, 1983,Pages 863-960.

19) Iverson R M. The physics of debris flows. Reviews of geophysics, 1997, 35(3): 245-296.

20) Iverson R M, Denlinger R P. Flow of variably fluidized granular masses across three-dimensional terrain: 1. Coulomb mixture theory. Journal of Geophysical Research: Solid Earth, 2001, 106(B1): 537-552.

21) Savage S B, Hutter K. The mobility of a finite mass of granular material down a rough incline. Journal of fluid mechanics, 1989, 199: 177-215.

22) Iverson R M, Reid M E, LaHusen R G. Debris-flow mobilization from landslides, Annu. Rev.

Earth Planet, 1997, 25, 85–138.

23) Iverson, R. M., and J. W. Vallance. New views of granular mass flows. Geology, 2001, 29, 115–118.

24) Iverson R M, Denlinger R P. Flow of variably fluidized granular masses across three-dimensional terrain: 1. Coulomb mixture theory. Journal of Geophysical Research: Solid Earth, 2001, 106(B1): 537-552.

25) Iverson R M. The debris-flow rheology myth[C]Debris flow Mechanics and Mitigation Conference, Mills Press, Davos. 2003: 303-314.

26) Iverson R M. Elements of an improved model of debris-flowmobility, in Powders and Grains 2009, pp. 9–16, Melville, New York.

27) Iverson R M, Reid M E, Logan M, et al. Positive feedback and momentum growth during debris-flow entrainment of wet bed sediment. Nature Geoscience, 2011, 4(2): 116.

28) Okura Y, Kitahara H, Ochiai H, et al. Landslide fluidization process by flume experiments. Engineering Geology, 2002, 66(1-2): 65-78.

29) Sassa K. mobility of landslides and debris flows -prediction of hazard area. Report for Grant-in-Aid for scientific research Project No. 61480062, Japanese Ministry on Education, Science and Culture, Tokyo, 1998, 4–52

30) Sassa K. Mechanisms of landslide triggered debris flows. Proceedings of IUFRO Division 8 Conference, 19–23 October 1998, Kyoto, 1998, 499–518

31) Sassa K. Mechanism of flows in granular soils. Proceedings of GeoEng2000, Melbourne, November 2000, 1671-1702

32) Sassa K, Fukuoka H, Wang G, et al. Undrained dynamic-loading ring-shear apparatus and its application to landslide dynamics, Landslides, 2004, 1:7–19

33) Huang Y, Dai Z L, Zhang W J, et al. SPH-based numerical simulations of flow slides in municipal solid waste landfills. Waste Manage Research, 2013, 31(3):256–264

34) Huang Y, Dai Z L. Large deformation and failure simulations for geo-disasters using smoothed particle hydrodynamics method. EngGeol, 2014, 168:86–97

35) Ahmadipur A, Qiu T, Sheikh B. Investigation of basal friction effects on impact force from a granular sliding mass to a rigid obstruction. Landslides, 2019.

36) Hungr O, Leroueil S, Picarelli L. The Varnes classification of landslide types, an update. Landslides, 2014, 11(2):167-194.

37) Yin Y, Sun P, Zhang M, et al. Mechanism on apparent dip sliding of oblique inclined bedding rockslide at Jiweishan, Chongqing, China. Landslides, 2011, 8(1):49-65.

38) Hungr O, Evans S G, Bovis M J, et al. A review of the classification of landslides of the flow type. Environmental & Engineering Geoscience, 2001, 7(3):221-238.

39) Yang, Wei, Wang, et al. Numerical Runout Modeling Analysis of the Loess Landslide at Yining, Xinjiang, China. Water, 2019, 11(7):1324.

40) Yang Gao, Yueping Yin, Bin Li, et al. Post-failure behavior analysis of the Shenzhen '12.20' CDW landfill landslide. Waste Management, 2019, 83(JAN.):171-183.

41) Johnson, A. M., Debris flow, in Slope Instability, edited by D. Brunsden and D. B. Prior, pp. 257–361, John Wiley, New York, 1984

42) Iverson R M, George D L. Modelling landslide liquefaction, mobility bifurcation and the dynamics of the 2014 Oso disaster. Géotechnique, 2016, 66(3):1-13.

43) Evett. I.W. On meaningful questions: a two-trace transfer problem. Journal of the Forensic Science Society,1987,27(6).

44) Jefferies M, Been K. Soil liquefaction: a critical state approach. CRC press, 2019.

45) Shi B, Wei J, Zhang Y. A novel experimental facility for measuring internal flow of Solid-liquid two-phase flow in a centrifugal pump by PIV. International Journal of Multiphase Flow, 2017, 89: 266-276.

46) Park Y C, Yoon C H, Lee D K, et al. Experimental studies on hydraulic lifting of solid-liquid two-phase flow. Ocean and Polar Research, 2004, 26(4): 647-653.

47) Peker S M, Helvaci S S. Solid-liquid two phase flow. Elsevier, 2011.

48) Thevand N, Daniel E. Numerical study of the lift force influence on two-phase shock tube boundary layer characteristics[J]. Shock Waves, 2002, 11(4): 279-288.

49) Zydak P, Klemens R. Modelling of dust lifting process behind propagating shock wave. Journal of Loss Prevention in the Process Industries, 2007, 20(4-6): 417-426

50) Anderson T B, Parnell J, Ruffell A H. Influence of basement on the geometry of Permo-Triassic basins in the northwest British Isles. Geological Society London Special Publications, 1995, 91(1):103-122.

51) Jackson R. The Dynamics of Fluidized Particles. 2000..

Figure 1 Schematic diagrams of our flume test model from the (a) side view and (b) top view perspectives. 1—hopper, 2—bracket, 3—flume bracket, 4—flume side plate, 5—flume bottom plate, 6—bottom plate, 7—front-view high-speed camera, 8—top-view high-speed camera, 9—lift engine, 10—side-view high-speed camera, 11—laser measuring instrument.

Figure 2 Sample slide materials. (a) Gravel pieces. (b) Clay particles. (c) Gravel and mud, which is a mixture of the gravel pieces, the clay particles, and water.

Figure 3 Side and front view of the results of (a) test T-01 (gravel), (b) test T-02 (gravel and mud), and test T-03 (mud).

Figure 4 Schematic diagrams of the top and side view of (a) test T-01 (gravel), (b) test T-02 (gravel and mud), and test T-03 (mud).

Figure 5 Velocity and acceleration data from tests T-01, T-02, and T-03.

Figure 6 Side and front views of the results of (a) test T-04 (gravel), (b) test T-05 (gravel and mud), and test T-06 (gravel and water).

Figure 7 Schematic diagrams of the top and side views of (a) test T-04 (gravel), (b) test T-05 (gravel and mud), and test T-06 (gravel and water).

Figure 8 Velocity and acceleration data from tests T-04, T-05, and T-06.

Figure 9 The drag effect exerted by the fluid phase in a two-phase flow.

528 **Table 1 Test schemes for our flume tests.**

Set no.	Test	Slide material	State	Carrier	Sliding inclination	Slide mass	Effect analysis
I	T-01	Dry gravel	Solid phase	None	20°	100 kg	Solid/liquid two-phase mobility characteristics
	T-02	Gravel and mud	Two-phase flow	Mud	20°	100 kg	
	T-03	Mud	Liquid phase	None	20°	100 kg	
II	T-04	Dry gravel	Solid phase	None	20°	200 kg	mobility characteristics of solid-liquid two-phase under the influences of different fluids
	T-05	Gravel and water	Two-phase flow	Water	20°	200 kg	
	T-06	Gravel and mud	Liquid phase	Mud	20°	200 kg	

529

Table 2 Results from the first set of flume tests.

Test	Slide medium	mobility distance	Maximum velocity	Maximum acceleration	Coefficient of friction	Force
T-01	Solid single-phase flow	120 cm	90 cm/s	90 cm/s^2	0.51	Solid shear
T-02	Fluid-solid two-phase flow	280 cm	120 cm/s	120 cm/s^2	0.43	Fluid drag
T-03	Fluid single-phase flow	380 cm	190 cm/s	190 cm/s^2	0.31	Fluid shear

532 Table 3 mobility and depositional data for the second set of flume tests.

Rheological model	mobility distance	Maximum velocity	Maximum acceleration	Coefficient of friction	Stage
T-04	180 cm	90 cm/s	90 cm/s^2	0.41	None
T-05	380 cm	170 cm/s	170 cm/s^2	0.3	Deceleration stage
T-06	580 cm	260 cm/s	200 cm/s^2	0.16	Acceleration stage

533

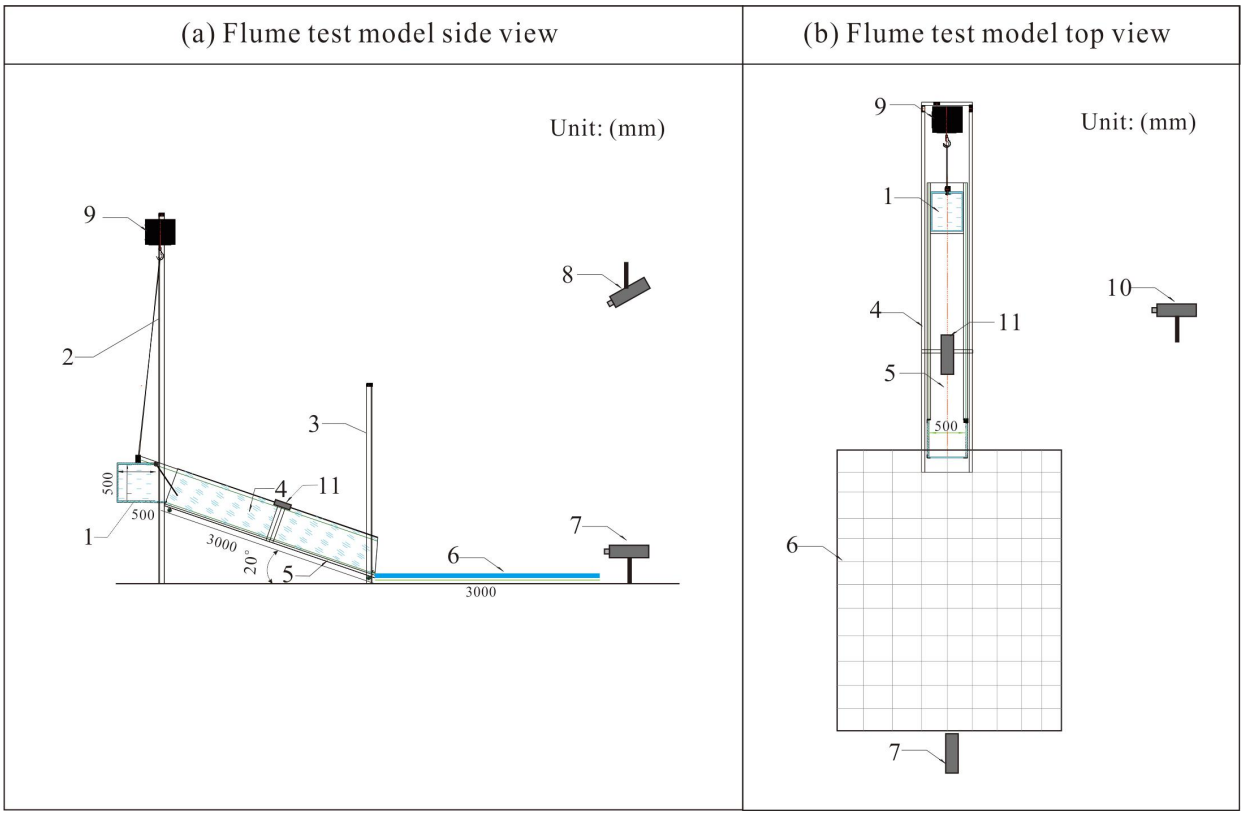
(a) Flume test model side view
(b) Flume test model top view
Unit: (mm)
Unit: (mm)
9
8
2
3
4
11
1
5
6
7
500
500
3000
20°
3000
9
1
10
4
11
5
500
6
7

Fig. 1

536

Fig.a Limestone gravel

Fig.b Fine-grained soil

Fig.c Gravel added viscous mud

537 Fig. 2

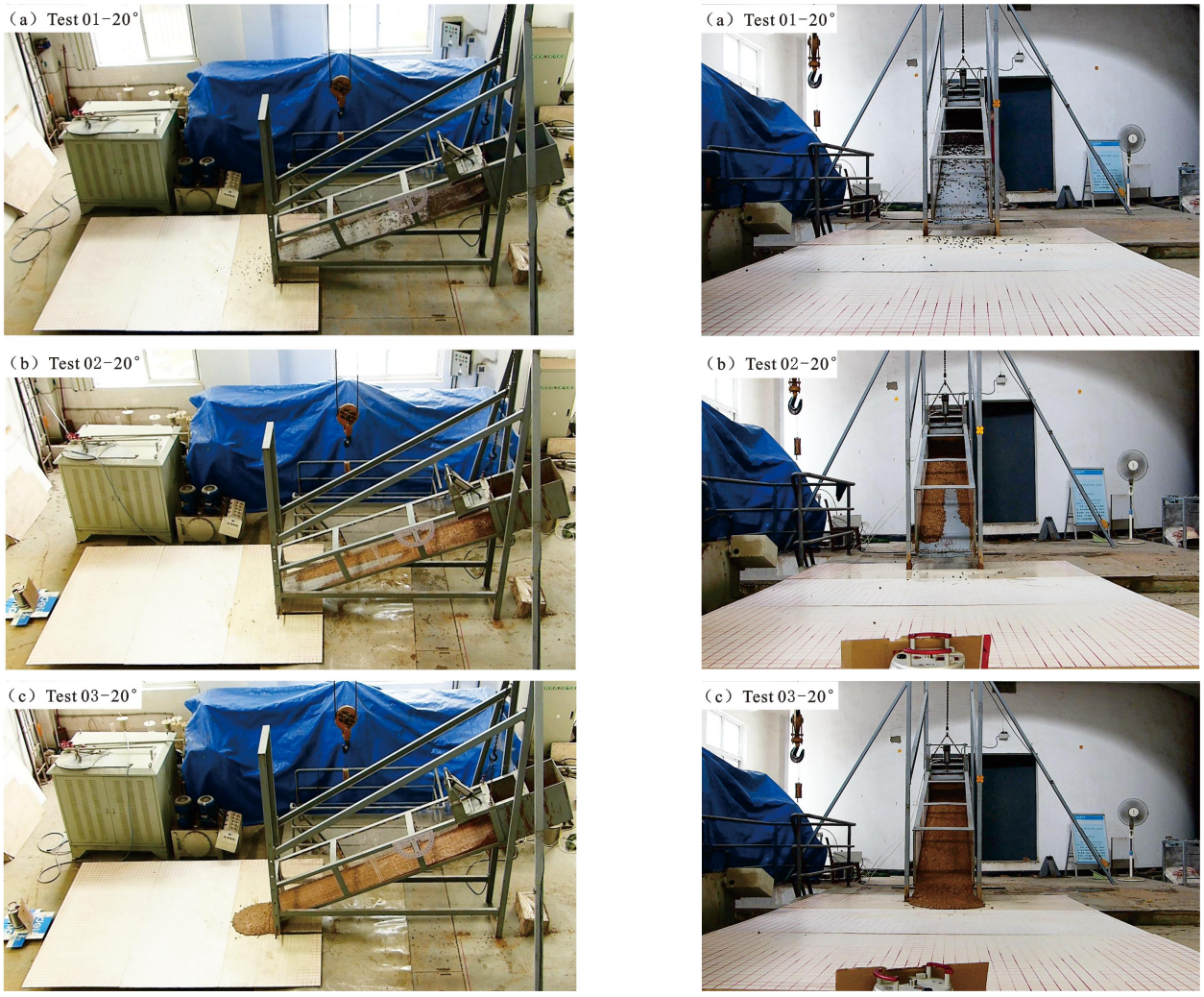
（a）Test 01-20°
（b）Test 02-20°
（c）Test 03-20°
（a）Test 01-20°
（b）Test 02-20°
（c）Test 03-20°

538

539 Fig. 3

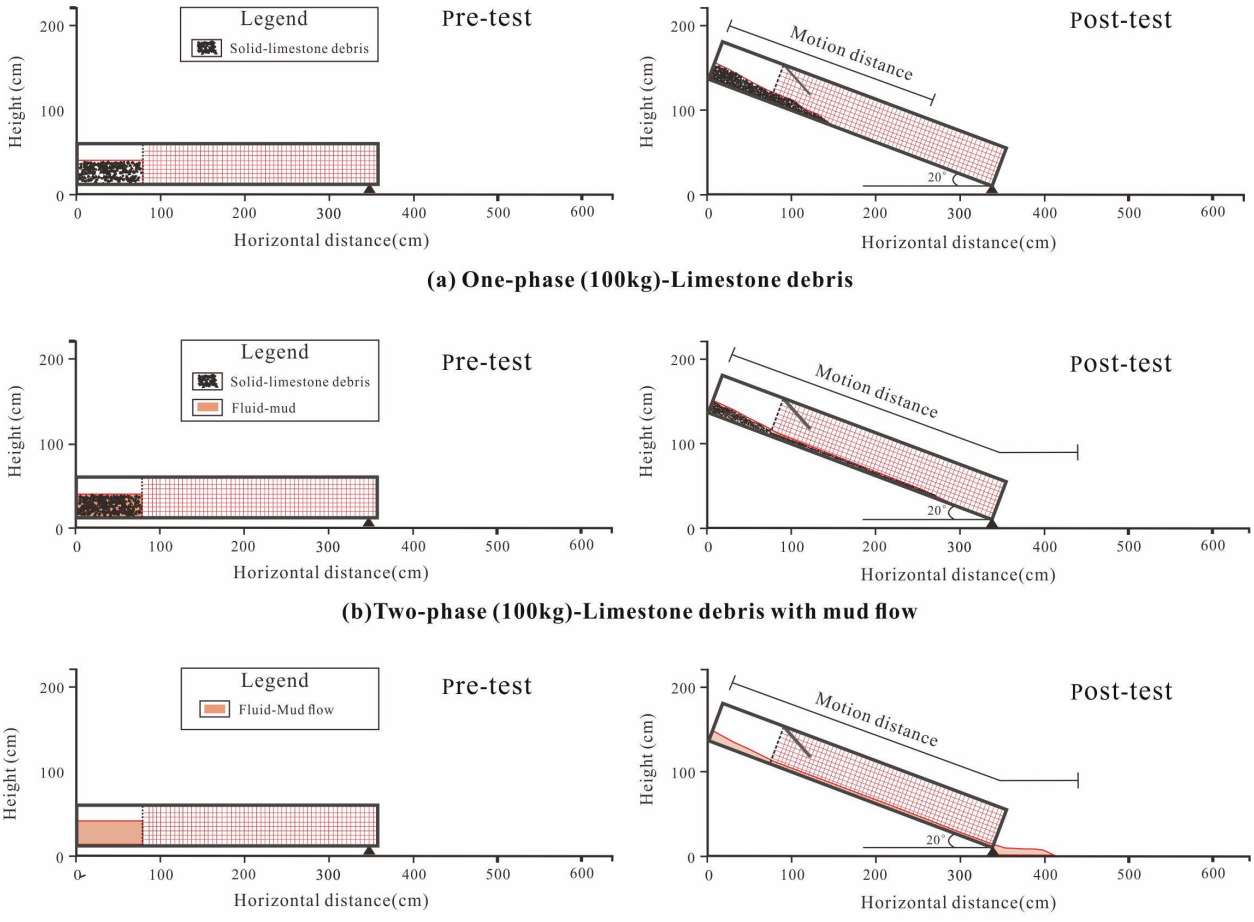
Legend
Solid-limestone debris
Pre-test
Post-test
Motion distance
Height (cm)
Horizontal distance(cm)
20°
(a) One-phase (100kg)-Limestone debris
Legend
Solid-limestone debris
Fluid-mud
Pre-test
Post-test
Motion distance
Height (cm)
Horizontal distance(cm)
20°
(b)Two-phase (100kg)-Limestone debris with mud flow
Legend
Fluid-Mud flow
Pre-test
Post-test
Motion distance
Height (cm)
Horizontal distance(cm)
20°
(c)One-phase (100kg)−Mud flow

Fig. 4

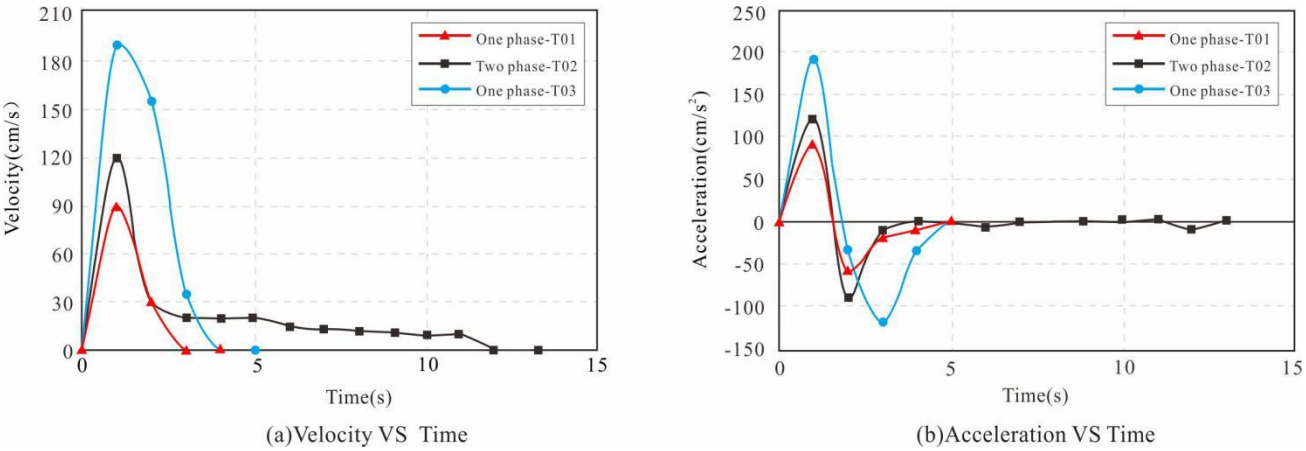

542 (a)Velocity VS Time (b)Acceleration VS Time

543 Fig. 5

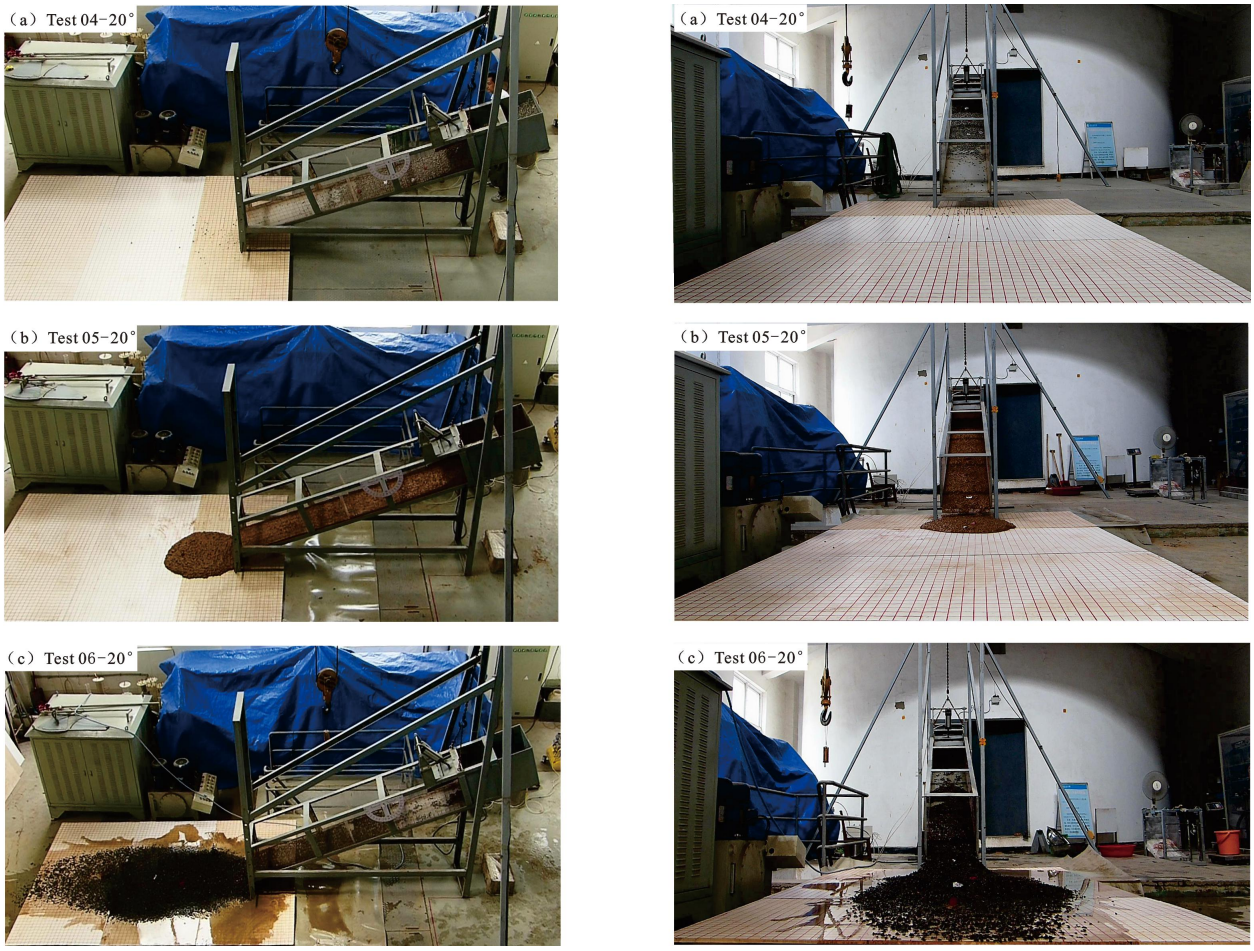
（a）Test 04-20°
（a）Test 04-20°
（b）Test 05-20°
（b）Test 05-20°
（c）Test 06-20°
（c）Test 06-20°

544

545 Fig. 6

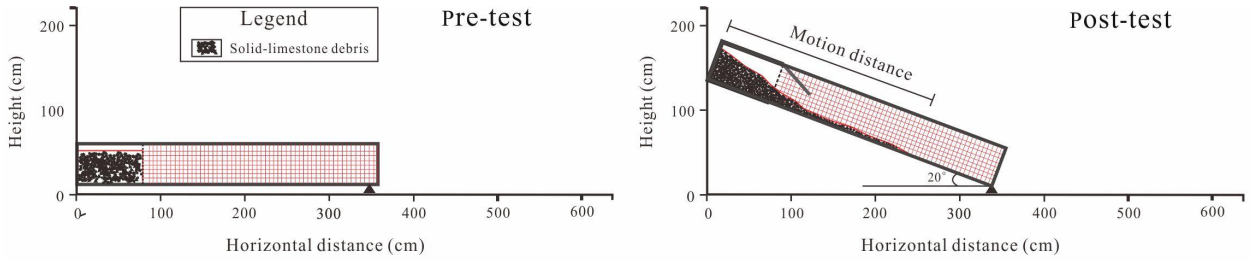

(a) One-Phase (200kg)-Limestone debris

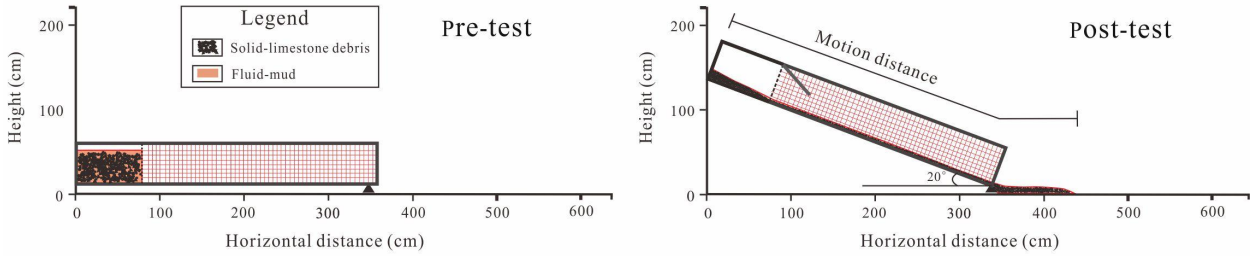

(b) Two-Phase (200kg)-Limestone debris and mud flow

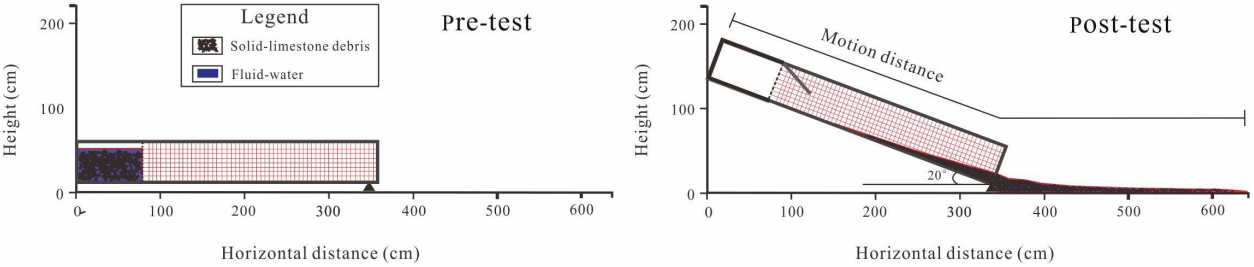

(c)Two-Phase (200kg)−Limestone debris and water flow

Fig. 7

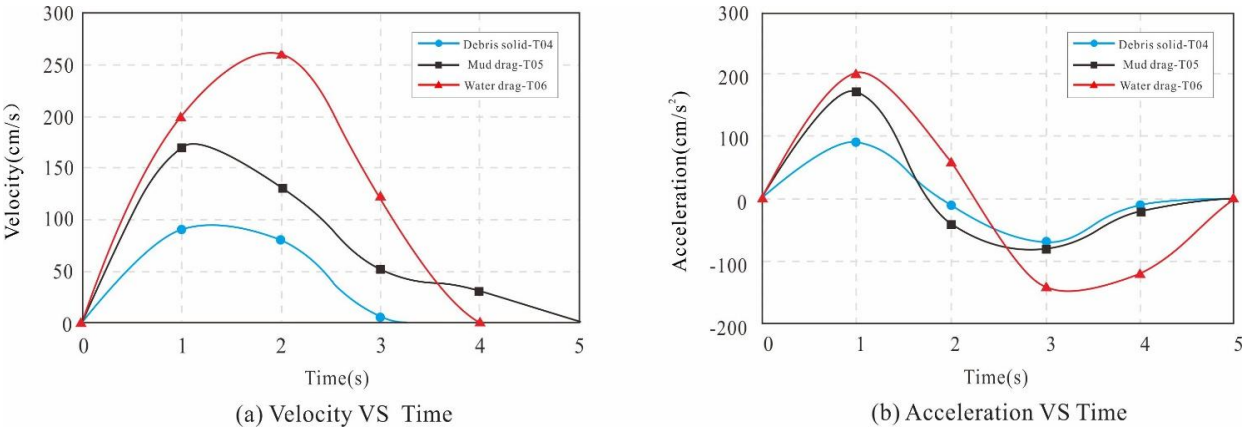

548 (a) Velocity VS Time (b) Acceleration VS Time

549 Fig. 8

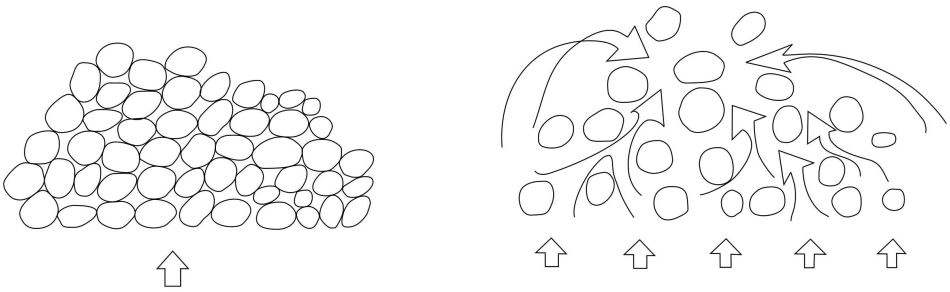

550 **(a) Dry gravel movement** **(b) two-phase movement**

551 Fig. 9